

# Binding of Catechols to Iron(III)–Octaethylporphyrin: An Experimental and DFT Investigation

Arvind Chaudhary,<sup>[a]</sup> Ranjan Patra,<sup>[a]</sup> and Sankar Prasad Rath\*<sup>[a]</sup>

*Dedicated to Prof. S. S. Krishnamurthy on the occasion of his 70th birthday*

**Keywords:** Catecholate binding / Hydrogen bonds / Spectroelectrochemistry / Density functional calculations / Structure elucidation

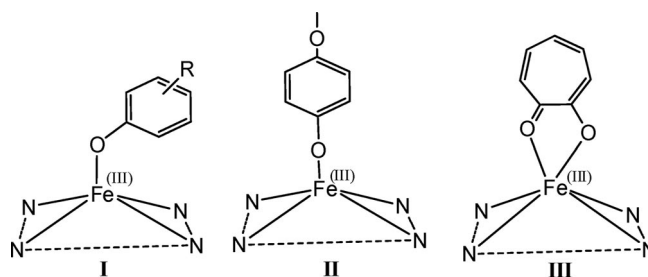
The synthesis, X-ray structure, and properties of high-spin, five-coordinate catecholate complexes of (octaethylporphyrinato)iron(III), Fe<sup>III</sup>(OEP)(L) (L: catecholate monoanion), are reported here for the first time. In these complexes, catechol binds in an  $\eta^1$ -fashion as an axial ligand, which is supported by DFT calculations. The Fe–O–C angles of Fe<sup>III</sup>(OEP)(Hcat), Fe<sup>III</sup>(OEP)(4-*t*Bu-Hcat), Fe<sup>III</sup>(OEP)(4-NO<sub>2</sub>-Hcat), and Fe<sup>III</sup>(OEP)(sal) are 119.5, 125.1, 122.2, and 124.3°, respectively. Fe<sup>III</sup>(OEP)(Hcat) has the smallest Fe–O–C angle in addition to the smallest dihedral angle of 26.2° between the planes of the porphyrin and axial catechol ligand among all phenolate complexes of iron(III)–porphyrins. In comparison to those of Fe<sup>III</sup>(OEP)(OPh) and Fe<sup>III</sup>(OEP)(4-*t*Bu-Hcat), the Fe–O bond in Fe<sup>III</sup>(OEP)(Hcat) is elongated by 0.064 and 0.038 Å,

respectively. This is due to the H-bonding interactions in Fe<sup>III</sup>(OEP)(Hcat) and not caused by steric hindrance. In the <sup>1</sup>H NMR spectra of the complexes, the signals of the *ortho*- and *para*-protons of catechol are shifted upfield, whereas those of the *meta*-protons are shifted downfield. The alternating shift pattern observed is due to negative and positive spin densities on the catechol carbon atoms and is indicative of  $\pi$ -spin delocalization on the catecholate ligand. Electrochemical data reveal that the complexes undergo three one-electron oxidations and a single one-electron reduction. Based on spectroelectrochemical and DFT studies, the first oxidation is assigned to a catechol-to-semiquinone transformation and the second and third oxidations are found to be porphyrin-ring-centered.

## Introduction

Catalase is a common enzyme found in nearly all living organisms exposed to oxygen, in which it catalyzes the decomposition of hydrogen peroxide to water and oxygen.<sup>[1–3]</sup> Catalase has one of the highest turnover numbers of all enzymes; one molecule of catalase can convert millions of molecules of hydrogen peroxide to water and oxygen. (Phenolato)(porphyrinato)iron(III) complexes merit attention on the basis of tyrosine coordination to (porphyrinato)iron(III) centers in catalase<sup>[1–7]</sup> and certain mutant hemoglobin. In case of catalase, the role of the axial phenolato ligand on the catalytic activity has been poorly investigated.<sup>[4]</sup> However, it is thought that the axial phenolato ligand must modulate the redox potential of the iron atom because of chemical similarity. Phenolato binding to Fe<sup>III</sup>–porphyrins has been known for quite some time as the  $\eta^1$ -O binding mode presented in **I**<sup>[8]</sup> and **II**.<sup>[9]</sup> The bidentate  $\eta^2$ -O,O binding of the tropolonate anion to iron–porphyrins, seen in **III**, has

also been reported.<sup>[10]</sup> The binding of benzene-1,2-diols (catechols) as substrates to the iron atom in nonheme enzymes, such as pyrochatechase and protocatechuate-3,4-dioxygenase, is well documented.<sup>[11]</sup> We sought to determine the nature of the binding of catechols with Fe<sup>III</sup>–porphyrins as no report on the structure and characterization of such species appears to exist. There are very few structural reports for catecholate-bound metalloporphyrins; just two examples are known with Sn<sup>IV</sup>–tetraphenylporphyrins<sup>[12a,12b]</sup> and one each with Zr<sup>IV</sup>–<sup>[12c]</sup> and Nb<sup>V</sup>–tetraphenylporphyrins.<sup>[12d]</sup>



This state of development has prompted us to undertake the task of binding catechols to Fe<sup>III</sup>–porphyrins. In the present work, we have successfully prepared stable cate-

[a] Department of Chemistry, Indian Institute of Technology Kanpur, Kanpur 208016, India  
E-mail: sprath@iitk.ac.in

Supporting information for this article is available on the WWW under <http://dx.doi.org/10.1002/ejic.201000707>.

cholate complexes of (octaethylporphyrinato)iron(III), which structurally mimic the active site of the resting state of catalase. Synthesis, structure, and properties of the new heme analogues  $\text{Fe}^{\text{III}}(\text{OEP})(\text{L})$  (L: Hcat, 4- $\text{NO}_2$ -Hcat and 4-*t*Bu-Hcat) are reported, in which catechol binds in an  $\eta^1$ -fashion as an axial ligand. The binding of salicylaldehyde to  $\text{Fe}^{\text{III}}$ -octaethylporphyrin has also been attempted, which also eventually yields  $\eta^1$ -coordination of the ligand. All the complexes reported here have been successfully characterized by single-crystal X-ray structure determinations. This study provides the basis for a discussion on the axial catecholate binding to iron-porphyrins especially regarding Fe–O bond character, Fe–O–C angle, and redox potential. Spectroelectrochemical investigations and density functional theory (DFT) calculations have been used to study various aspects of the electronic structures of the complexes.

## Results and Discussion

The free octaethylporphyrin ( $\text{H}_2\text{OEP}$ ) and  $[\text{Fe}^{\text{III}}(\text{OEP})_2\text{O}]$  were prepared according to literature procedures.<sup>[13]</sup> A solution of  $[\text{Fe}^{\text{III}}(\text{OEP})_2\text{O}]$  with excess L (L:  $\text{H}_2\text{cat}$ , 4- $\text{NO}_2$ - $\text{H}_2\text{cat}$ , 4-*t*Bu- $\text{H}_2\text{cat}$ , and Hsal) in THF was heated to reflux to form  $\text{Fe}^{\text{III}}(\text{OEP})(\text{L})$ , which after cooling to room temperature was concentrated to complete dryness. From a solution of this residue, dark brown crystals of the product were deposited by slow diffusion. The crystals were collected by filtration and structurally characterized. Scheme 1 shows the synthetic strategy and list of the complexes reported in the paper along with their abbreviations.

The UV/Vis spectrum of  $\text{Fe}^{\text{III}}(\text{OEP})(\text{Hcat})$  in chloroform shows a Soret band at 391 nm and three Q-bands at 500, 529, and 612 nm. Similar spectral features are also observed in the other complexes reported here. Under similar condi-

tions, the previously reported five-coordinate  $\text{Fe}^{\text{III}}(\text{OEP})(\text{OPh})$  shows a Soret band at 391 and three Q-bands at 490, 520, and 603 nm, which suggests a coordination number of five for the complexes reported here.<sup>[8a,14]</sup> In our complexes, the positions of the charge-transfer band (around 600–650 nm) and Soret band (around 390 nm) are found to be dependent on the acidity of the axial ligand. For example, the addition of an electron-donating substituent (*t*Bu) to the catechol redshifts the Soret band of the complex to 393 nm, whereas the charge-transfer band blueshifts to 608 nm. The reverse trends are obtained by adding an electron-withdrawing ( $\text{NO}_2$ ) substituent onto the catechol.

EPR measurements show similar spectral features in both solid and solution state; Figure 1 shows two representative spectra of the complexes. Both spectra are axially symmetric for  $\text{Fe}^{\text{III}}(\text{OEP})(\text{Hcat})$  with  $g_{\perp} = 5.96$  and  $g_{\parallel} = 2.01$  for the frozen toluene solution and  $g_{\perp} = 5.97$  and  $g_{\parallel} = 1.99$  for the powder. The solution magnetic moment for

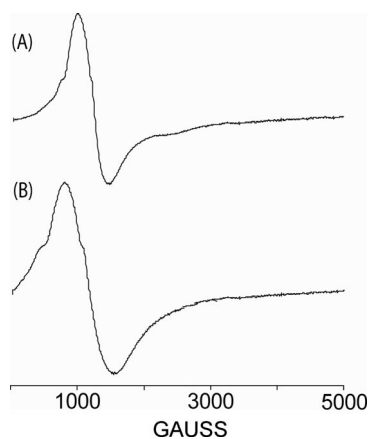
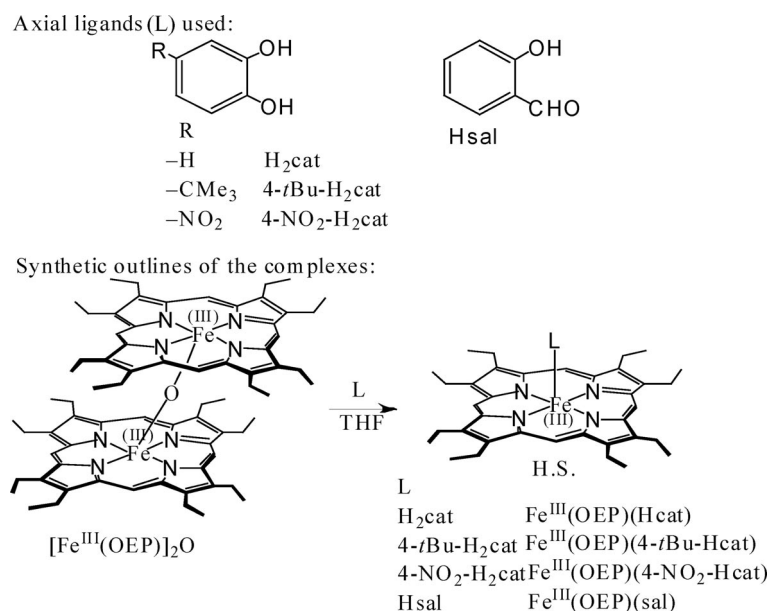


Figure 1. X-band EPR spectrum recorded in toluene (at 120 K) of (A)  $\text{Fe}^{\text{III}}(\text{OEP})(\text{Hcat})$  and (B)  $\text{Fe}^{\text{III}}(\text{OEP})(4\text{-}t\text{Bu-Hcat})$ .



Scheme 1.

Fe<sup>III</sup>(OEP)(Hcat) at 295 K in purified dichloromethane, calculated by Evan's method,<sup>[15]</sup> was found to be 5.91 BM. Similar results are obtained for the other iron(III)-catecholate complexes. These results suggest high-spin states of iron ( $S = 5/2$ ) in both solid and solution phase for all of the complexes.

### Crystallographic Characterization of Fe<sup>III</sup>(OEP)(Hcat)

Dark brown crystals of Fe<sup>III</sup>(OEP)(Hcat) were obtained from the slow diffusion of acetonitrile into a THF solution of the complex in air in the presence of a slight excess of H<sub>2</sub>cat. The molecule crystallizes in the triclinic crystal system with a  $P\bar{1}$  space group, and a perspective view is shown in Figure 2. This is the first structural characterization of the binding of catechols to Fe<sup>III</sup>-porphyrins. In the asymmetric unit, one full molecule of the complex along with one free catechol molecule is present. Selected bond lengths and angles are given in Table 1. The complex has a five-coordinate square-pyramidal geometry, in which the iron atom is displaced by 0.42 Å from the N<sub>4</sub> plane of the porphyrin ring, a distance within the range of 0.39–0.54 Å and seen for other high-spin five-coordinate iron(III)-porphyrins.<sup>[8]</sup> The average Fe–N and Fe–O distances are found to be 2.059(2) and 1.912(1) Å, respectively. The Fe–O–C bond angle is 119.5(1)°, which is the smallest angle reported for any phenolato complex of Fe<sup>III</sup>-porphyrin. It is worth noting that the Fe–O–C bond angle for Fe<sup>III</sup>(OEP)(OPh) is 142.2(3)°.<sup>[8a]</sup>

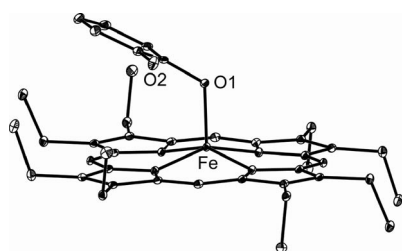


Figure 2. A perspective view of Fe<sup>III</sup>(OEP)(Hcat) showing 50% thermal contours for all non-hydrogen atoms at 100 K (H atoms have been omitted for clarity).

Figure 3a displays aspects of H-bonding interactions between oxygen atoms of the coordinated and free catechol molecules in the crystal lattice. The hydrogen atoms bound to catecholate oxygen atoms in the structure are directly located in difference Fourier maps, whereas all other protons were added in calculated positions. The catecholate oxygen atom O1 is engaged in H-bonding interactions with O3 of the free catechol molecule present in the asymmetric unit. The uncoordinated catechol oxygen atom O2 also forms H-bonds with O4 of the symmetry-related catechol molecule. Catechol oxygen atoms are also engaged in H-bonding interactions with the symmetry-related catechol molecule forming a dimer, which eventually bridges between two iron-porphyrins in the crystal lattice. Thus, three types of H-bonds are observed: O(4)⋯H–O(2), O(1)⋯H–O(3), and O(4)⋯H–O(3), and these distances are 2.928(2),

Table 1. Selected bond lengths [Å] and angles [°] for Fe<sup>III</sup>(OEP)(L).

L:	Fe <sup>III</sup> (OEP)(L)			
	Hcat	4- <i>t</i> Bu-Hcat	4-NO <sub>2</sub> -Hcat	sal
Fe1–N1	2.0645(17)	2.075(3)	2.058(3)	2.058(3)
Fe1–N2	2.0576(18)	2.055(3)	2.052(4)	2.063(3)
Fe1–N3	2.0603(17)	2.069(3)	2.057(4)	2.065(3)
Fe1–N4	2.0551(18)	2.055(3)	2.052(4)	2.058(3)
Fe1–O1	1.9120(14)	1.874(2)	1.909(3)	1.912(3)
N(1)–Fe–N(2)	87.61(7)	88.26(10)	87.76(13)	87.18(12)
N(1)–Fe–N(3)	156.81(7)	159.04(10)	156.44(15)	154.79(13)
N(1)–Fe–N(4)	87.41(7)	87.59(10)	87.58(14)	87.53(12)
N(2)–Fe–N(3)	87.55(7)	87.85(11)	87.60(15)	87.26(12)
N(2)–Fe–N(4)	155.71(7)	157.41(10)	157.06(15)	154.91(13)
N(3)–Fe–N(4)	87.74(7)	88.14(10)	87.75(14)	87.16(12)
N(1)–Fe–O(1)	101.66(6)	100.64(9)	104.76(14)	100.04(12)
N(2)–Fe–O(1)	103.34(7)	100.42(10)	100.11(14)	101.90(12)
N(3)–Fe–O(1)	101.53(7)	100.31(10)	98.80(14)	105.16(12)
N(4)–Fe–O(1)	100.95(7)	102.17(10)	102.79(14)	103.17(12)
Fe–O1–C37	119.48(13)	125.13(19)	122.2(3)	124.3(4)

2.616(2), and 2.705(2) Å, respectively. A bond of the latter type generates a dimer between two free catechol molecules, whereas the first two types connect between coordinated and free catechol molecules in the crystal lattice. Figure 3b shows the packing diagram for Fe<sup>III</sup>(OEP)(Hcat).

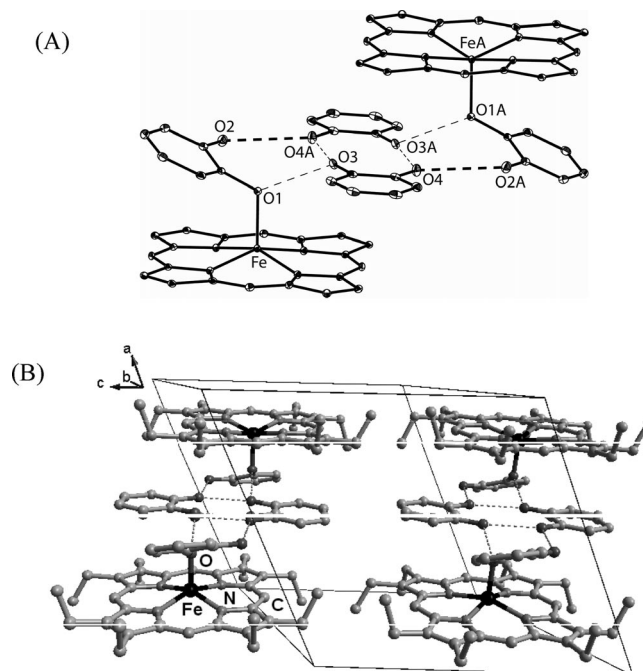


Figure 3. (A) Hydrogen-bonding interactions between Fe<sup>III</sup>(OEP)(Hcat) and free catechol molecules in the crystal lattice (hydrogen atoms and ethyl substituents are omitted for clarity). (B) Crystal packing diagram of Fe<sup>III</sup>(OEP)(Hcat).

### Crystallographic Characterization of Fe<sup>III</sup>(OEP)(4-*t*Bu-Hcat)

Dark brown crystals of Fe<sup>III</sup>(OEP)(4-*t*Bu-Hcat) were grown by slow diffusion of cyclohexane into a tetrahydrofuran solution of the complex in the presence of a

slight excess of 4-*t*Bu-H<sub>2</sub>cat in air at room temperature. The molecule crystallizes in the triclinic crystal system with a  $P\bar{1}$  space group, and the asymmetric unit contains one full molecule of the complex. A perspective view of Fe<sup>III</sup>-(OEP)(4-*t*Bu-Hcat) is shown in Figure 4, and selected bond lengths and angles are given in Table 1. The average Fe–N and Fe–O bond lengths are 2.063(3) and 1.874(2) Å, respectively, and the Fe–O–C angle is 125.1(2)°. The uncoordinated OH group of the *tert*-butylcatechol has orientational disorder and is distributed between two possible *ortho* sites with 62% and 38% occupancies. The occupancies were determined by refinement, and the refined occupancies were then fixed in subsequent cycles of refinement.

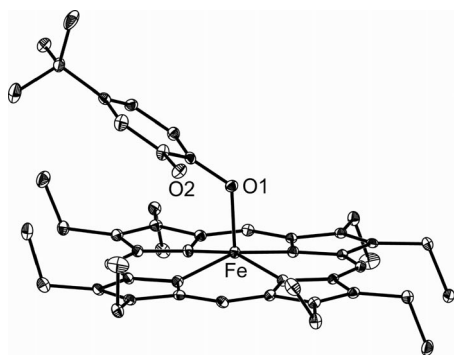


Figure 4. A perspective view of Fe<sup>III</sup>(OEP)(4-*t*Bu-Hcat) showing 50% thermal contours for all non-hydrogen atoms at 100 K (H-atoms have been omitted for clarity).

### Crystallographic Characterization of Fe<sup>III</sup>(OEP)(4-NO<sub>2</sub>-Hcat)

Dark brown crystals of Fe<sup>III</sup>(OEP)(4-NO<sub>2</sub>-Hcat) were grown by slow diffusion of cyclohexane into a chloroform solution of the complex in the presence of a slight excess of 4-NO<sub>2</sub>-H<sub>2</sub>cat at room temperature in air. The complex crystallizes in the monoclinic crystal system with a  $C2/c$  space group, and the asymmetric unit contains one full molecule of the complex. The iron atom binds in an  $\eta^1$ -fashion with either of the two hydroxy groups of 4-nitrocatechol, but to an unequal extent. As a result, the nitro and the uncoordinated hydroxy groups have two possible orientations with 85 and 15% occupancies. These two possible coordination modes of 4-NO<sub>2</sub>-Hcat are also seen in solution (*vide infra*). A perspective view of the molecule is shown in Figure 5, and selected bond lengths and angles are given in Table 1. The Fe–N distances are in the narrow range of 2.052–2.058 Å and the Fe–O distance is 1.909(3). These distances fall within the spread of literature values observed for high-spin iron(III) porphyrinates containing axial phenoxido ligands.<sup>[8]</sup> The complex has a five-coordinate square-pyramidal geometry, in which the iron atom is displaced by 0.41 Å from the N<sub>4</sub> plane of the porphyrin ring, a distance in the range of 0.39–0.54 Å and seen for other high-spin five-coordinate iron(III)–porphyrins.<sup>[8]</sup>

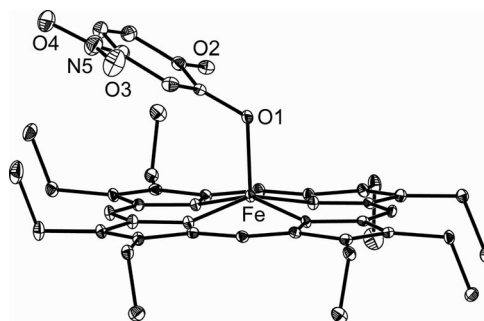


Figure 5. Perspective view of Fe<sup>III</sup>(OEP)(4-NO<sub>2</sub>-Hcat) showing 50% thermal contours for all non-hydrogen atoms at 100 K (H-atoms have been omitted for clarity). Only the major orientation of 4-nitrocatechol is shown.

### Crystallographic Characterization of Fe<sup>III</sup>(OEP)(sal)

Dark brown crystals of Fe<sup>III</sup>(OEP)(sal) were grown by slow diffusion of hexane into a THF solution of the complex in the presence of a slight excess of salicylaldehyde at room temperature in air. The complex crystallizes in the monoclinic space group  $C2/c$ , and a perspective view is shown in Figure 6. The average Fe–N bond length is 2.061(3) Å, and the Fe–O distance is 1.912(3) Å. The Fe–O–C angle of 124.3(4)° is similar to that previously reported for Fe<sup>III</sup>–porphyrins coordinated with phenols.<sup>[8]</sup> Salicylaldehyde can bind with the iron atom in two possible modes and thus has orientational disorder with 54.4 and 45.6% occupancies. The occupancies were originally determined by refinement, which was then fixed in subsequent cycles of refinement.

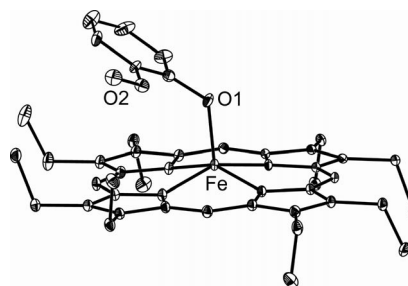


Figure 6. Perspective view of Fe<sup>III</sup>(OEP)(sal) showing 50% thermal contours for all non-hydrogen atoms at 100 K (H-atoms have been omitted for clarity). Only the major orientation of salicylaldehyde is shown.

Several structurally characterized iron(III) porphinate complexes with phenolato ligands have been reported previously.<sup>[8,10]</sup> Table 2 compares the key structural parameters of these complexes along with the catecholato complexes reported here. As seen from the table, Fe<sup>III</sup>(OEP)(Hcat) has the smallest Fe–O–C angle and the smallest dihedral angle between the planes of the porphyrin and the axial catechol ligand among all phenolato complexes of iron(III)–porphyrins reported so far. The average Fe–N distance increases in the order: Fe<sup>III</sup>(OEP)(4-NO<sub>2</sub>-Hcat) < Fe<sup>III</sup>(OEP)(Hcat) < Fe<sup>III</sup>(OEP)(4-*t*Bu-Hcat), whereas the Fe–O

Table 2. Selected geometric parameters for phenoxido complexes of Fe<sup>III</sup>–porphyrins.

Complex	Fe–N <sup>[a]</sup>	Fe–O <sup>[b]</sup>	Fe–O–C <sup>[c]</sup>	ΔFe <sub>4N</sub> <sup>[d]</sup>	ϕ <sup>[e]</sup>	Ref.
Fe <sup>III</sup> (OEP)(Hcat)	2.059(2)	1.912(1)	119.5(3)	0.42	26.2	this work
Fe <sup>III</sup> (OEP)(4- <i>t</i> Bu-Hcat)	2.063(3)	1.874(2)	125.1(2)	0.39	34.6	this work
Fe <sup>III</sup> (OEP)(4-NO <sub>2</sub> -Hcat)	2.054(4)	1.909(3)	122.2(3)	0.41	31.4	this work
Fe <sup>III</sup> (OEP)(sal)	2.061(3)	1.912(3)	124.3(4)	0.44	32.9	this work
Fe <sup>III</sup> (OEP)(OPh)	2.061	1.848(4)	142.2(3)	0.47	96	[8a]
Fe <sup>III</sup> (OEP){O-2,6-(CF <sub>3</sub> CONH) <sub>2</sub> C <sub>6</sub> H <sub>3}}</sub>	2.051	1.926(3)	122.8(3)	0.43	28.7	[8a]
Fe <sup>III</sup> (OEP)(O-2-CF <sub>3</sub> CONHC <sub>6</sub> H <sub>4</sub> )	2.060	1.887(2)	125.5(2)	0.44	39.2	[8a]
Fe <sup>III</sup> (OEP){O-2,6- <i>i</i> Pr <sub>2</sub> C <sub>6</sub> H <sub>3}}</sub>	2.071	1.816(4)	170.6(4)	0.48	81.7	[8a]
Fe <sup>III</sup> (TPP)(O-2,2'-Cl <sub>2</sub> C <sub>6</sub> H <sub>3</sub> )	2.059	1.868	132.54	0.46	39.9	[8d]
Fe <sup>III</sup> (OEP)(tropolone)	2.122	2.067	120.75	0.69	87	[10]
		2.064	120.50			
Fe <sup>III</sup> (TPP)(O-2-CF <sub>3</sub> CONHC <sub>6</sub> H <sub>4</sub> )	2.071	1.847(5)	146.0(5)	0.44	73.3	[8b]
Fe <sup>III</sup> (TPP)(OPh)·C <sub>6</sub> H <sub>6</sub>	2.077	1.842	129.97	0.47	34.9	[8c]
Fe <sup>III</sup> (TPP)(OPh)·C <sub>7</sub> H <sub>8</sub>	2.103	1.842	132.92	0.58	39.9	[8c]
Fe <sup>III</sup> (TPP)(O-2-ClC <sub>6</sub> H <sub>4</sub> )	2.093	1.896	126.99	0.58	38.5	[8c]

[a] Average value in Å. [b] Value in Å. [c] Value in °. [d] Displacement of the iron atom from the mean plane containing the four porphyrin nitrogen atoms in Å. [e] Dihedral angle between the plane of the porphyrin (24 atoms) and the axial ligand.

distance decreases in the same order with an exception in the case of Fe<sup>III</sup>(OEP)(Hcat), in which the Fe–O distance is the longest.

It is appropriate to compare Fe<sup>III</sup>(OEP)(Hcat) and Fe<sup>III</sup>(OEP)(OPh) since the former only has an additional uncoordinated OH group. However, their X-ray structures reveal that Fe<sup>III</sup>(OEP)(Hcat) is engaged in H-bonding between oxygen atoms of coordinated and free catechol. Compared with those of Fe<sup>III</sup>(OEP)(OPh) and Fe<sup>III</sup>(OEP)(4-*t*Bu-Hcat), the Fe–O bond in Fe<sup>III</sup>(OEP)(Hcat) is elongated by 0.064 and 0.038 Å, respectively. The elongation of the Fe–O distance is certainly due to the H-bonding interactions and not caused by steric hindrance. The IR stretching frequencies for OH of Fe<sup>III</sup>(OEP)(Hcat) and free H<sub>2</sub>cat were observed at 3440 and 3451 cm<sup>-1</sup> respectively. This shift of ν(O–H) (11 cm<sup>-1</sup>) supports the presence of O–H⋯O hydrogen bonds observed by X-ray analysis. In contrast to the large Fe–O–C bond angle of 142.2(3)° for Fe<sup>III</sup>(OEP)(OPh), the Fe–O–C angles of Fe<sup>III</sup>(OEP)(Hcat), Fe<sup>III</sup>(OEP)(4-*t*Bu-Hcat), Fe<sup>III</sup>(OEP)(4-NO<sub>2</sub>-Hcat), and Fe<sup>III</sup>(OEP)(sal) are 119.5, 125.1, 122.2, and 124.3°, respectively. The relatively small Fe–O–C angles observed are notable since a small Fe–O–C bond angle is unsuitable for orbital overlap. In addition, such remarkable bending is not forced by crystal packing or H-bonding [with the exception of Fe<sup>III</sup>(OEP)(Hcat) where H-bonding is present], and thus the coordinated oxygen atom must have reduced s-character. In contrast, the smaller Fe–O–C bond angles for Fe<sup>III</sup>(OEP)[O-2,6-(CF<sub>3</sub>CONH)<sub>2</sub>C<sub>6</sub>H<sub>3</sub>] and Fe<sup>III</sup>(OEP)(O-2-CF<sub>3</sub>CONHC<sub>6</sub>H<sub>4</sub>) are explained by their NH⋯O H-bonds.<sup>[8a]</sup>

### <sup>1</sup>H NMR Study

<sup>1</sup>H NMR spectra of CDCl<sub>3</sub> solutions of the Fe<sup>III</sup>(OEP)(L) complexes were obtained at 295 K and are shown in Figure 7. The signals are broad, and the chemical shifts,

which are temperature-dependent, are shifted both upfield and downfield indicative of π-spin delocalization. It is expected that there should be one *meso* resonance, two methylene resonances, and one methyl resonance for five-coordinate Fe<sup>III</sup>(OEP)(L). As seen in Figure 7 and Table 3, the two methylene peaks arise in the narrow downfield region between δ = 35 and 46 ppm, the lone *meso* signal is observed in the upfield region at δ ≈ -37 ppm. The resonances for the methyl protons are found in the diamagnetic region at δ ≈ 6.5 ppm since they are far from the paramagnetic Fe

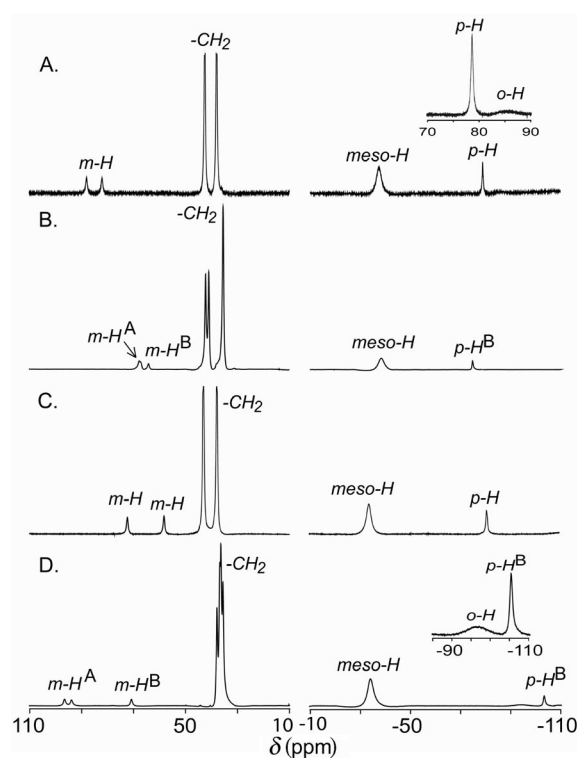


Figure 7. <sup>1</sup>H NMR spectra at 295 K of CDCl<sub>3</sub> solutions of (A) Fe<sup>III</sup>(OEP)(sal), (B) Fe<sup>III</sup>(OEP)(4-NO<sub>2</sub>-Hcat), (C) Fe<sup>III</sup>(OEP)(Hcat), and (D) Fe<sup>III</sup>(OEP)(4-*t*Bu-Hcat).

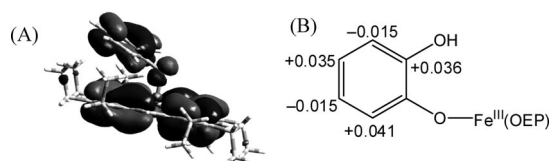
Table 3.  $^1\text{H}$  NMR chemical shifts of  $\text{Fe}^{\text{III}}(\text{OEP})(\text{L})$  measured in  $\text{CDCl}_3$  at 295 K.

Complex	<i>m</i> -H	<i>p</i> -H	<i>o</i> -H	<i>meso</i>	$\text{CH}_2$	$\text{CH}_3$
$\text{Fe}^{\text{III}}(\text{OEP})(\text{Hcat})$	74.5, 58.6	-80.5	[a]	-33.8	38.2, 43.4	6.4
$\text{Fe}^{\text{III}}(\text{OEP})(4-t\text{Bu-Hcat})$	96.7 (A), 94.2 (A), 70.8 (B)	-107.6 (B)	-98.5	-35.7	37.9, 36.8, 36.4, 35.6	5.8
$\text{Fe}^{\text{III}}(\text{OEP})(4-\text{NO}_2\text{-Hcat})$	67.7 (A), 67.3 (A), 64.2 (B)	-74.6 (B)	[a]	-38.1	42.5, 41.2, 35.9	5.7
$\text{Fe}^{\text{III}}(\text{OEP})(\text{sal})$	80.4, 76.4	-78.5	-85.5	-36.8	40.3, 36.3	6.9

[a] Not detected.

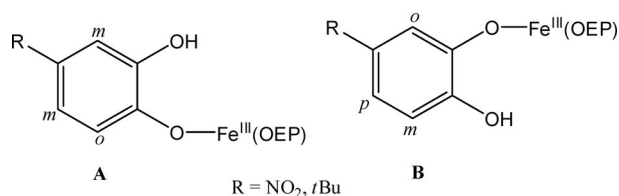
centre. For a typical five-coordinate high-spin complex of  $\text{Fe}^{\text{III}}(\text{OEP})\text{Cl}$ , the  $^1\text{H}$  NMR spectrum in  $\text{CDCl}_3$  comprises two methylene resonance at  $\delta = 40.9$  and  $44.4$  ppm and one *meso* resonance at  $\delta = -56.8$  ppm.<sup>[16]</sup> Chemical shifts of the  $\text{CH}_3$  protons of the peripheral ethyl substituent are also sensitive to spin states;  $S = 5/2$  complexes exhibit the  $\text{CH}_3$  signals further downfield, because the unpaired electrons can be delocalized through  $\sigma$ -bonds.<sup>[17]</sup> Thus, the positioning of the methyl, methylene, and *meso* signals provide more evidence for the high-spin ( $S = 5/2$ ) nature of the complexes in solution.<sup>[17,18]</sup>

Molecular orbital calculations of  $\text{Fe}^{\text{III}}(\text{OEP})(\text{Hcat})$  by using DFT<sup>[19]</sup> clearly show that the electron spin densities are also spread over the catechol ligand (Figure 8a). Figure 8b shows the Mulliken spin densities of the catechol carbon atoms of the complex, in which the spin densities are positive at *ortho* and *para* positions and negative at the *meta* position. Thus, the *ortho*- and *para*-protons show upfield shifts, whereas *meta*-protons show downfield shifts. The alternating shift pattern, which is the opposite sign of the chemical shifts for *meta*- vs. *ortho*- and *para*-protons, is also indicative of  $\pi$ -spin delocalization on the catecholato ligand. The *ortho*-protons of the axial catechol ligand are closest to the paramagnetic Fe centre and have extremely small  $T_1$  (spin-lattice relaxation time) values because of the dipolar contact from the high-spin  $\text{Fe}^{\text{III}}$  ion. As a result, signals arising from the *ortho*-protons are very broad, and some of them could not be located. Similar observations are also reported where thiolates are used as axial ligands.<sup>[20]</sup>

Figure 8. (A) Singly occupied HOMO of  $\text{Fe}^{\text{III}}(\text{OEP})(\text{Hcat})$  and (B) Mulliken spin densities of the catechol carbon atoms.

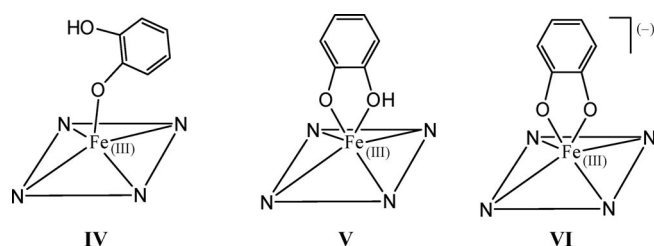
In complexes with catechol, the iron center can bind either of the two available oxygen atoms, and therefore two  $^1\text{H}$  NMR peaks in the downfield region are observed from the two *meta*-protons, whereas one signal in the upfield region arises from the *para*-proton. For substituted catechols, the iron center also can bind with either of the two catechol oxygen atoms as shown in Scheme 2. As a result of the substitution, the two forms become inequivalent, which can be seen in the X-ray structure of the molecule in the solid (vide supra) as well as in solution. For form A, two  $^1\text{H}$  NMR

signals in the downfield region are observed from the two nonequivalent *meta*-protons. However, for form B, one downfield and one upfield proton resonance are observed due to one *meta*- and one *para*-proton, respectively. Signals arising from the *ortho*-protons are too broad to be observed. Figure 7b and d show the  $^1\text{H}$  NMR spectra of  $\text{Fe}^{\text{III}}(\text{OEP})(4-\text{NO}_2\text{-Hcat})$  and  $\text{Fe}^{\text{III}}(\text{OEP})(4-t\text{Bu-Hcat})$  at 295 K, in which A and B can be identified easily, and the resonances are listed in Table 3.



Scheme 2.

Catechol can bind to iron(III)-porphyrins in the monodentate  $\eta^1\text{-O}$  binding mode (IV), the bidentate mononegative  $\eta^2\text{-O,O}$  binding mode (V), and the bidentate binegative  $\eta^2\text{-O,O}$  binding mode (VI), shown in Scheme 3. When catechol binds in the  $\eta^2$ -fashion in any six-coordinate  $\text{Fe}^{\text{III}}$  complex, bite angles are observed within the narrow range of  $80\text{--}85^\circ$ .<sup>[12c,12d,21]</sup> The  $\eta^2$ -binding of tropolone with  $\text{Fe}^{\text{III}}$ -porphyrin is the only known example, in which the bite angle was found to be outside this range ( $73^\circ$ ).<sup>[10]</sup> For the  $\text{Fe}^{\text{III}}$ -porphyrins reported here, catechol only binds in the  $\eta^1$ -fashion. To bind catechol in the  $\eta^2$ -binding mode (as in V and VI) the bite angles need to be increased, which also increases the repulsion further. Single-point energy calculations have been performed by using DFT for all probable binding modes of catechol (Scheme 3) in  $\text{Fe}^{\text{III}}(\text{OEP})(\text{Hcat})$ . For the  $\eta^1$ -coordination mode (IV), atom coordinates were taken directly from the single-crystal X-ray structure of the molecule. However, for the  $\eta^2$ -coordination modes (V and



Scheme 3.

VI), the atom coordinates were taken from the single-crystal X-ray structure of  $\text{Fe}^{\text{III}}(\text{OEP})(\text{tropolone})^{[10]}$  with the required change in the bite angle of catechol. The calculation shows that the  $\eta^1$ -binding mode of catechol (IV), as observed in the X-ray structure of  $\text{Fe}^{\text{III}}(\text{OEP})(\text{Hcat})$ , is found to be energetically much more favorable than the two  $\eta^2$ -binding modes (V and VI).

Very few structural reports of catecholato-bound metalloporphyrins exist. Two examples of the  $\eta^1$ -binding mode of catechol have been observed for  $\text{Sn}^{\text{IV}}$ -tetraphenylporphyrins in a six-coordinate species.<sup>[12a,12b]</sup> Two more examples have been reported where the catechol oxygen atom binds the metal center in both  $\eta^1$ - and  $\eta^2$ -modes to form seven-coordinate species, one with  $\text{Zr}^{\text{IV}}$ -tetraphenylporphyrin<sup>[12c]</sup> and other with  $\text{Nb}^{\text{V}}$ -tetraphenylporphyrin.<sup>[12d]</sup> In both cases, the larger size of the metal ions as well as very large metal displacements from the mean porphyrin plane (1.06 and 1.02 Å, respectively) facilitate the  $\eta^2$ -binding mode and the increase in coordination number.<sup>[12c,12d]</sup>

### Cyclic Voltammetric Study

Cyclic voltammetric experiments were carried out at 25 °C under nitrogen in  $\text{CH}_2\text{Cl}_2$  with 0.1 M tetrabutylammonium hexafluorophosphate (TBAH) as the supporting electrolyte. Two representative cyclic voltammograms are shown in Figures 9 and S1 (see Supporting Information), and the potentials are given in the Experimental Section. Electrochemical data reveal that the complexes undergo three one-electron oxidations and a single one-electron reduction. The first oxidation is assigned to the catechol-to-semiquinone oxidation, and the second and third oxidations are porphyrin-ring-centered (vide infra) and quasi-reversible under the experimental conditions.

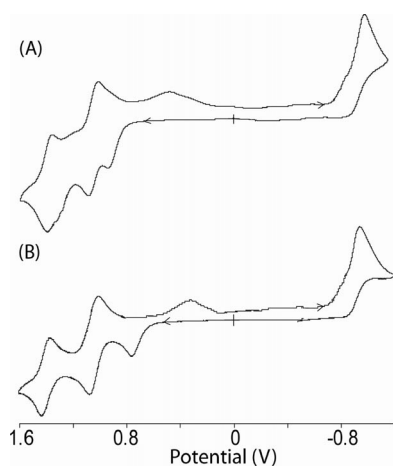


Figure 9. Cyclic voltammograms of (A)  $\text{Fe}^{\text{III}}(\text{OEP})(4\text{-NO}_2\text{-Hcat})$  and (B)  $\text{Fe}^{\text{III}}(\text{OEP})(4\text{-}t\text{Bu-Hcat})$  in  $\text{CH}_2\text{Cl}_2$  (scan rate 100 mV/s) with 0.1 M TBAH as the supporting electrolyte and  $\text{Ag}/\text{AgCl}$  as the reference electrode.

### Spectroelectrochemical Study

Bulk oxidation of dichloromethane solutions of  $\text{Fe}^{\text{III}}(\text{OEP})(\text{L})$  at a constant potential under nitrogen have been performed. The gradual UV/Vis spectral change during the 1e-oxidation process is shown for  $\text{Fe}^{\text{III}}(\text{OEP})(4\text{-}t\text{Bu-Hcat})$  in Figure 10, in which the intensities of Soret and charge-transfer bands at 392 and 615 nm, respectively, decrease in intensity, whereas the corresponding peaks at 380 and 638 nm increase in intensity. Similar spectral changes are also observed for the other complexes and are assigned to the catechol-to-semiquinone oxidation based on previously reported observations.<sup>[8f]</sup> Solid- and solution-phase IR spectra of the complexes were recorded before and after the oxidation. The 1265 and 1422  $\text{cm}^{-1}$  bands are assigned to the  $\nu(\text{CO})$  bands of  $\text{Fe}^{\text{III}}(\text{OEP})(4\text{-}t\text{Bu-Hcat})$  and the 1e-oxidized species, respectively. The  $\nu(\text{CO})$  bands of  $\text{M}(\text{cat})$  and  $\text{M}(\text{sq})$  complexes generally appear in the ranges of 1250–1275 and 1400–1500  $\text{cm}^{-1}$ , respectively.<sup>[22]</sup> According to these criteria, the  $\nu(\text{CO})$  band of the 1e-oxidized species is assigned to the semiquinone, which is further justified by our DFT calculations (vide infra).

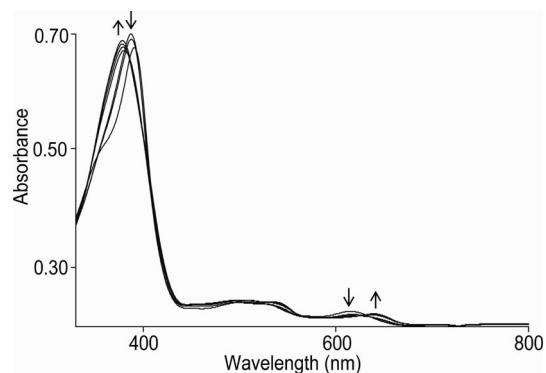


Figure 10. UV/Vis spectra in  $\text{CH}_2\text{Cl}_2$  during the 1e-oxidation of  $\text{Fe}^{\text{III}}(\text{OEP})(4\text{-}t\text{Bu-Hcat})$ , with an applied potential of 0.75 V. Arrows indicate the increase and decrease of band intensity.

2e-Oxidations of  $\text{Fe}^{\text{III}}(\text{OEP})(\text{L})$  at a fixed anodic potential under nitrogen have also been performed, during which the initial brown solution changed to green. Figure 11 shows the UV/Vis spectral change of  $\text{Fe}^{\text{III}}(\text{OEP})(4\text{-NO}_2\text{-Hcat})$  upon oxidation at a constant potential of 1.28 V, in which the Soret band at 386 nm blueshifts to 357 nm with a decrease in intensity and generates a porphyrin dication,  $[\text{Fe}^{\text{III}}(\text{OEP})(\text{L})]^{++}$ , which is confirmed by DFT. These spectral changes are characteristic of the presence of a porphyrin  $\pi$ -cation radical.<sup>[23]</sup> Similar spectral features are also observed during the controlled oxidations of the other complexes reported here. Molecular orbital calculations have been performed by using DFT for both the 1e- and 2e-oxidized products of  $\text{Fe}^{\text{III}}(\text{OEP})(\text{Hcat})$ . The HOMOs of both of the oxidized species are presented in Figure 12, which clearly demonstrates the removal of the first electron mostly from the catechol part of the molecule, whereas the second electron is removed from the porphyrin ring, as observed experimentally.

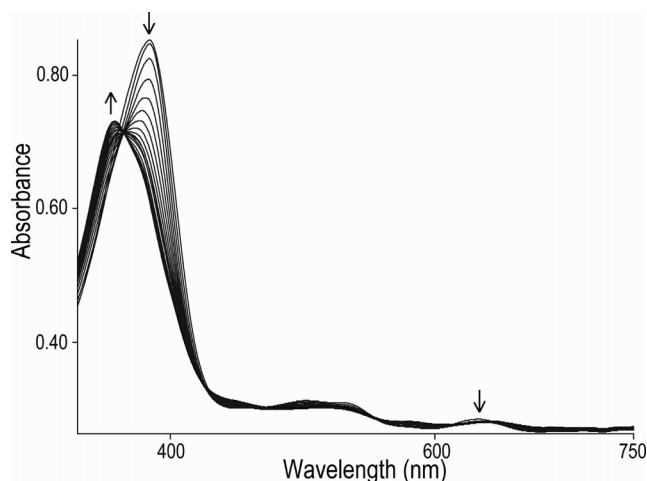


Figure 11. UV/Vis spectra in  $\text{CH}_2\text{Cl}_2$  during the 2e-oxidations of  $\text{Fe}^{\text{III}}(\text{OEP})(4\text{-NO}_2\text{-Hcat})$ , with an applied potential of 1.28 V. Arrows indicate the increase and decrease of band intensity.

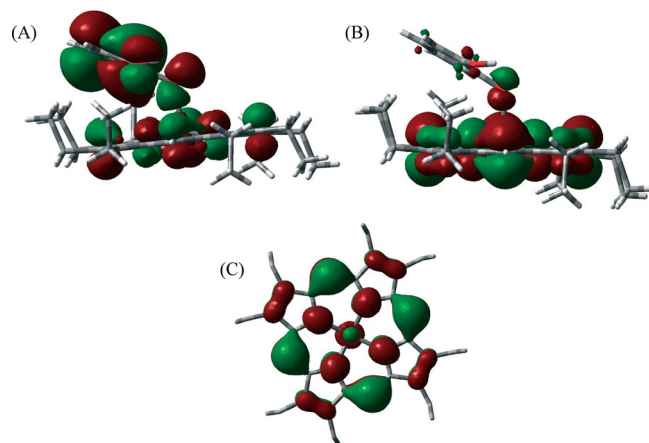


Figure 12. Singly occupied HOMOs of (A)  $[\text{Fe}^{\text{III}}(\text{OEP})(\text{Hcat})]^{\bullet+}$ ; (B)  $[\text{Fe}^{\text{III}}(\text{OEP})(\text{Hcat})]^{2+}$ , and (C) porphyrin macrocycle of  $[\text{Fe}^{\text{III}}(\text{OEP})(\text{Hcat})]^{2+}$  showing both  $A_{1u}$  and  $A_{2u}$  contributions.

Ghosh and co-workers applied DFT to investigate the energetics, molecular structures, and spin-density profiles of metalloporphyrin  $\pi$ -cation radicals.<sup>[24c]</sup> Metallo-OEP (OEP = octaethylporphyrin) derivatives form  $A_{1u}$ -type cation radicals, whereas metallo-TPP (TPP = *meso*-tetraphenylporphyrin) derivatives form  $A_{2u}$ -type cation radicals.<sup>[24]</sup> The common practice of describing these radicals in terms of the  $A_{1u}/A_{2u}$  dichotomy is often not justified, because the actual picture is further complicated by the pseudo-Jahn–Teller effect.<sup>[24d]</sup> Interestingly, it was concluded that not all metalloporphyrin  $\pi$ -cation radicals are subject to pseudo-Jahn–Teller distortion. For example, by employing energy-difference criteria, it was suggested that metallooctaethylporphyrin should always be pseudo-Jahn–Teller-distorted, whereas metallo-*meso*-tetrahalogenoporphyrin radicals should be not.<sup>[24a]</sup> The pseudo-Jahn–Teller distortion leads to structures with lower symmetries and mixed character with respect to the  $A_{1u}$  and  $A_{2u}$  components. Our DFT

study of  $[\text{Fe}(\text{OEP})(\text{Hcat})]^{2+}$  shows that the HOMO also has a mixed character with both  $A_{1u}$  and  $A_{2u}$  generated from pseudo-Jahn–Teller distortion (Figure 12c).

## Conclusions

Synthesis, X-ray structures, and properties of new heme analogues  $\text{Fe}^{\text{III}}(\text{OEP})(\text{L})$  (L: Hcat, 4- $\text{NO}_2$ -Hcat, 4-*t*Bu-Hcat, and sal) are reported, in which catechol binds in an  $\eta^1$ -fashion as an axial ligand. DFT calculations show that the  $\eta^1$ -binding mode, as observed in the X-ray structure, is energetically much more favorable than the  $\eta^2$ -binding modes.  $\text{Fe}^{\text{III}}(\text{OEP})(\text{Hcat})$  has the smallest Fe–O–C angle of  $119.5(1)^\circ$  and the smallest dihedral angle of  $26.2^\circ$  between the planes of the porphyrin and the axial catechol ligand of all phenolato complexes of iron(III)–porphyrins reported. In comparison with those of  $\text{Fe}^{\text{III}}(\text{OEP})(\text{OPh})$  and  $\text{Fe}^{\text{III}}(\text{OEP})(4\text{-}i\text{Bu-Hcat})$ , the Fe–O bond length in  $\text{Fe}^{\text{III}}(\text{OEP})(\text{Hcat})$  is elongated by 0.064 and 0.038 Å, respectively, which is due to the H-bonding interactions with the coordinated catechol oxygen atom and not steric hindrance. The solid- and solution-state spectral observations are characteristic of high-spin complexes. In the  $^1\text{H}$  NMR spectra, the signals of the *ortho*- and *para*-protons of the catechol ligands are shifted upfield, whereas those of the *meta*-protons are shifted downfield. The alternating shift pattern, which has the opposite sign of the chemical shifts for *meta*-vs. *ortho*- and *para*-protons, is due to negative and positive spin densities on the catecholate carbon atoms and is also indicative of  $\pi$ -spin delocalization. The iron center can bind with either catechol oxygen atom, which is observed in both solid- and solution-state investigations. Electrochemical data reveal that the complexes undergo three one-electron oxidations and a single one-electron reduction. The first oxidation is assigned as the catechol-to-semiquinone oxidation and the second and third oxidations are porphyrin-ring-centered. These assignments are further supported by theoretical calculations. Spectroelectrochemical and DFT studies have been used to assign the electronic structures of the oxidized species.

## Experimental Section

**Materials:** Reagents and solvents were purchased from commercial sources and purified according to standard procedures before use. Grade-I neutral alumina was used for column chromatography.  $\text{H}_2\text{OEP}$  was prepared according to a literature method,<sup>[13a]</sup> and iron was inserted by a reported procedure under an inert gas, which produced the corresponding  $\text{Fe}^{\text{III}}(\text{OEP})\text{Cl}$  in excellent yield.<sup>[25]</sup>  $[\text{Fe}^{\text{III}}(\text{OEP})]_2\text{O}$  was prepared as described previously.<sup>[13b]</sup> The complexes  $\text{Fe}^{\text{III}}(\text{OEP})(\text{L})$  were prepared according to a general method; details are given below for a representative case.

**Preparation of  $\text{Fe}^{\text{III}}(\text{OEP})(\text{Hcat})\text{-H}_2\text{cat}$ :**  $[\text{Fe}(\text{OEP})]_2\text{O}$  (100 mg, 0.082 mmol) was dissolved in tetrahydrofuran (25 mL). Catechol (45 mg, 0.41 mmol) in tetrahydrofuran (5 mL) was added, and the mixture was heated under  $\text{N}_2$  to reflux for 2 h. As the reaction proceeded, the greenish-red solution changed to dark brown. After completion of the reaction, the solution was cooled and concen-

trated to complete dryness to obtain a dark brown solid. The resulting solid was dissolved in tetrahydrofuran and layered with acetonitrile at room temperature in air. After standing for 7–8 d, dark brown crystalline solids of  $\text{Fe}^{\text{III}}(\text{OEP})(\text{Hcat})\cdot\text{H}_2\text{cat}$  had deposited, which were collected by filtration and dried. Yield: 43 mg, 70%.  $\text{C}_{48}\text{H}_{55}\text{FeN}_4\text{O}_4$  (807.36): calcd. C 71.40, H 6.86, N 6.94; found C 71.49, H 6.95, N 6.89. UV/Vis (chloroform):  $\lambda_{\text{max}}$  ( $\epsilon$ ) = 391 ( $1.6 \times 10^5$ ), 500 ( $1.73 \times 10^4$ ), 529 ( $1.65 \times 10^4$ ), 612 ( $9.86 \times 10^3 \text{ M}^{-1} \text{ cm}^{-1}$ ) nm. IR (KBr):  $\tilde{\nu}$  = 3440 (OH)  $\text{cm}^{-1}$ . EPR (120 K): solid:  $g_{\perp}$  = 5.97,  $g_{\parallel}$  = 1.99; solution:  $g_{\perp}$  = 5.96,  $g_{\parallel}$  = 2.01.  $E_{1/2}(\text{ox})$  = 0.88, 1.11, 1.44 V;  $E_{1/2}(\text{red})$  =  $-0.80 \text{ V}$ .  $\mu_{\text{eff}}$  (295 K, in  $\text{CH}_2\text{Cl}_2$ ) =  $5.91 \mu_{\text{B}}$ .

The following compounds were prepared by using similar procedures.

**Preparation of  $\text{Fe}^{\text{III}}(\text{OEP})(4\text{-NO}_2\text{-Hcat})$ :** Yield: 47 mg, 80%.  $\text{C}_{42}\text{H}_{48}\text{FeN}_5\text{O}_4$  (742.30): calcd. C 67.95, H 6.51, N 9.43; found C 67.87, H 6.60, N 9.35. UV/Vis (chloroform):  $\lambda_{\text{max}}$  ( $\epsilon$ ) = 389 ( $2.54 \times 10^5$ ), 499 ( $2.54 \times 10^4$ ), 527 ( $2.52 \times 10^4$ ), 621 ( $1.4 \times 10^4 \text{ M}^{-1} \text{ cm}^{-1}$ ) nm. IR (KBr):  $\tilde{\nu}$  = 3462 (OH)  $\text{cm}^{-1}$ . EPR (120 K): solid:  $g_{\perp}$  = 5.96,  $g_{\parallel}$  = 2.01; solution:  $g_{\perp}$  = 5.98,  $g_{\parallel}$  = 1.99.  $E_{1/2}(\text{ox})$ : 0.93, 1.08, 1.43 V;  $E_{1/2}(\text{red})$ :  $-0.94 \text{ V}$ .  $\mu_{\text{eff}}$  (295 K, in  $\text{CH}_2\text{Cl}_2$ ) =  $5.94 \mu_{\text{B}}$ .

**Preparation of  $\text{Fe}^{\text{III}}(\text{OEP})(4\text{-}t\text{Bu-Hcat})$ :** Yield: 46 mg, 75%.  $\text{C}_{46}\text{H}_{57}\text{FeN}_4\text{O}_2$  (753.38): calcd. C 73.33, H 7.62, N 7.43; found C 73.22, H 7.54, N 7.38. UV/Vis (chloroform):  $\lambda_{\text{max}}$  ( $\epsilon$ ) = 393 ( $2.26 \times 10^5$ ), 496 ( $2.24 \times 10^4$ ), 526 ( $2.18 \times 10^4$ ), 608 ( $1.36 \times 10^4 \text{ M}^{-1} \text{ cm}^{-1}$ ) nm. IR (KBr):  $\tilde{\nu}$  = 3438 (OH)  $\text{cm}^{-1}$ . EPR (120 K): solid:  $g_{\perp}$  = 5.95,  $g_{\parallel}$  = 2.01; solution:  $g_{\perp}$  = 5.97,  $g_{\parallel}$  = 1.99.  $E_{1/2}(\text{ox})$  = 0.75, 1.12, 1.44 V;  $E_{1/2}(\text{red})$  =  $-0.73 \text{ V}$ .  $\mu_{\text{eff}}$  (295 K, in  $\text{CH}_2\text{Cl}_2$ ) =  $5.93 \mu_{\text{B}}$ .

**Preparation of  $\text{Fe}^{\text{III}}(\text{OEP})(\text{sal})$ :** Yield: 59 mg, 90%.  $\text{C}_{43}\text{H}_{49}\text{FeN}_4\text{O}_2$  (709.32): calcd. C 72.81, H 6.96, N 7.89; found C 72.75, H 7.08, N 7.82. UV/Vis (chloroform)  $\lambda_{\text{max}}$  ( $\epsilon$ ) = 394 ( $2.5 \times 10^5$ ), 495 ( $1.9 \times 10^4$ ), 526 ( $1.8 \times 10^4$ ), 613 ( $9.92 \times 10^3$ ). IR (KBr):  $\tilde{\nu}$  = 1723 (CO)  $\text{cm}^{-1}$ . EPR (120 K): solid:  $g_{\perp}$  = 5.95,  $g_{\parallel}$  = 2.01; solution:  $g_{\perp}$

= 5.97,  $g_{\parallel}$  = 1.99.  $E_{1/2}(\text{ox})$  = 0.94, 1.42 V;  $E_{1/2}(\text{red})$  =  $-0.85 \text{ V}$ .  $\mu_{\text{eff}}$  (295 K, in  $\text{CH}_2\text{Cl}_2$ ) =  $5.95 \mu_{\text{B}}$ .

**Instrumentation:** UV/Vis spectra were recorded with a PerkinElmer UV/Vis spectrometer. Elemental (C, H, and N) analyses were performed with a CE-440 elemental analyzer. IR spectra were recorded in the range 4000–400  $\text{cm}^{-1}$  with a Bruker Vertex 70 Spectrophotometer. EPR spectra were obtained with a Bruker EMX EPR spectrometer. Cyclic voltammetric studies were performed with a BAS Epsilon electrochemical workstation in dichloromethane with 0.1 M TBAH as the supporting electrolyte, Ag/AgCl as the reference electrode, and Pt wire as the auxiliary electrode. The concentration of the compounds was in the order of  $10^{-3} \text{ M}$ . The ferrocene/ferrocenium couple occurs at  $E_{1/2}(\Delta E_{\text{p}}) = +0.45 \text{ V}$  (65 mV) vs. Ag/AgCl under the same experimental conditions.  $^1\text{H}$  NMR spectra were recorded with a JEOL 500 MHz instrument. The spectra for paramagnetic molecules were recorded over a 100 kHz bandwidth with 64 K data points and a  $5 \mu\text{s}$   $90^\circ$  pulse. For a typical spectrum between 2000 and 3000 transients were accumulated with a 50 ms delay time. The residual  $^1\text{H}$  resonances of the solvents were used as a secondary reference.

**X-ray Structure Solution and Refinement:** Crystals were coated with light hydrocarbon oil and mounted in the 100 K dinitrogen stream of a Bruker SMART APEX CCD diffractometer equipped with a CRYO Industries low-temperature apparatus, and intensity data were collected by using graphite-monochromated Mo- $K_{\alpha}$  radiation ( $\lambda = 0.71073 \text{ \AA}$ ). The data integration and reduction were processed with SAINT<sup>[26]</sup> software. An absorption correction was applied.<sup>[27]</sup> Structures were solved by direct methods using SHELXS-97 and were refined on  $F^2$  with full-matrix least-squares techniques by using the SHELXL-97 program package.<sup>[28]</sup> Non-hydrogen atoms were refined anisotropically. In the refinement, hydrogen atoms were treated as riding atoms by using SHELXL default parameters. Crystal data and data collection parameters are given in Table 4. CCDC-782059, -782058, -782061, and -782060 contain the supplementary crystallographic data for this paper. These data can be

Table 4. Crystal data and data collection parameters.

	$\text{Fe}^{\text{III}}(\text{OEP})(\text{Hcat})$	$\text{Fe}^{\text{III}}(\text{OEP})(4\text{-}t\text{Bu-Hcat})$	$\text{Fe}^{\text{III}}(\text{OEP})(4\text{-NO}_2\text{-Hcat})$	$\text{Fe}^{\text{III}}(\text{OEP})(\text{sal})$
$T$ [K]	100(2)	100(2)	100(2)	100(2)
Empirical formula	$\text{C}_{48}\text{H}_{55}\text{FeN}_4\text{O}_4$	$\text{C}_{46}\text{H}_{57}\text{FeN}_4\text{O}_2$	$\text{C}_{42}\text{H}_{48}\text{FeN}_5\text{O}_4$	$\text{C}_{43}\text{H}_{49}\text{FeN}_4\text{O}_2$
Formula mass	807.81	753.81	742.70	709.32
Crystal system	triclinic	triclinic	monoclinic	monoclinic
Space group	$P\bar{1}$	$P\bar{1}$	$C2/c$	$C2/c$
$a$ [ $\text{\AA}$ ]	12.6927(8)	12.388(2)	21.0337(18)	20.624(5)
$b$ [ $\text{\AA}$ ]	13.6188(9)	13.315(2)	20.9809(18)	21.201(5)
$c$ [ $\text{\AA}$ ]	13.7795(9)	14.035(2)	16.7705(14)	16.897(5)
$\alpha$ [ $^\circ$ ]	66.3110(10)	100.138(3)	90	90
$\beta$ [ $^\circ$ ]	68.6410(10)	110.308(3)	95.940(2)	98.296(5)
$\gamma$ [ $^\circ$ ]	84.7360(10)	104.825(3)	90	90
$V$ [ $\text{\AA}^3$ ]	2027.2(2)	2007.2(6)	7361.2(11)	7311(3)
Radiation	Mo- $K_{\alpha}$	Mo- $K_{\alpha}$	Mo- $K_{\alpha}$	Mo- $K_{\alpha}$
$\lambda$ [ $\text{\AA}$ ]	0.71073	0.71073	0.71073	0.71073
$Z$	2	2	8	4
$d_{\text{calcd.}}$ [ $\text{g cm}^{-3}$ ]	1.323	1.247	1.340	1.290
$\mu$ [ $\text{mm}^{-1}$ ]	0.423	0.418	0.460	0.455
$F(000)$	858	806	3144	3016
No. of unique data	7420	7337	8572	6777
No. of parameters refined	531	495	493	508
GOF on $F^2$	1.008	1.035	1.014	1.077
$R1^{\text{[a]}}$ [ $T > 2\sigma(I)$ ]	0.0457	0.0615	0.0785	0.0714
$R1^{\text{[a]}}$ (all data)	0.0535	0.0833	0.1492	0.1080
$wR2^{\text{[b]}}$ (all data)	0.1168	0.1582	0.2103	0.1924

[a]  $R1 = \sum ||F_o| - |F_c|| / \sum |F_o|$ . [b]  $\{\sum [w(F_o^2 - F_c^2)^2] / \sum [w(F_o^2)^2]\}^{1/2}$ .

obtained free of charge from The Cambridge Crystallographic Data Centre via [www.ccdc.cam.ac.uk/data\\_request/cif](http://www.ccdc.cam.ac.uk/data_request/cif).

**Computational Details:** DFT calculations were performed with a B3LYP hybrid functional by using the Gaussian 03, revision B.04, package.<sup>[19]</sup> The method used was Becke's three-parameter hybrid exchange functional,<sup>[29]</sup> the nonlocal correlation was provided by the Lee, Yang, and Parr expression,<sup>[30]</sup> and the Vosko, Wilk, and Nuair 1980 correlation functional (III) for local correction. The basis set was LanL2DZ for the iron atom and 6-31G\*\* for the carbon, nitrogen, oxygen, and hydrogen atoms. Molecular orbital calculations were performed for  $[\text{Fe}^{\text{III}}(\text{OEP})(\text{Hcat})]^+$  and  $[\text{Fe}^{\text{III}}(\text{OEP})(\text{Hcat})]^{2+}$  where all the coordinates were taken directly from the single-crystal X-ray structure of  $\text{Fe}^{\text{III}}(\text{OEP})(\text{Hcat})$ . Single-point energy calculations were performed for  $\text{Fe}^{\text{III}}(\text{OEP})(\text{Hcat})$ , in which the mode of catechol binding with Fe varies between **IV**, **V**, and **VI** as shown in Scheme 3. For the  $\eta^1$ -coordination mode (**IV**), the atom coordinates are taken directly from the single-crystal X-ray structure of the molecule. However, for the  $\eta^2$ -binding modes (**V** and **VI**), the atom coordinates are taken from the single-crystal X-ray structure of  $\text{Fe}^{\text{III}}(\text{OEP})(\text{tropolone})$ ,<sup>[10]</sup> tropolone was replaced by catechol, and the bite angle was fixed manually at 82°. For the binategative  $\eta^2$ -coordination mode (**VI**), negative charge was balanced by a hydronium ion. The total energy was calculated by simply adding the energy obtained for **VI** with the energy of the hydronium ion. For **IV** and **V**, however, the total energy was adjusted by adding the energy of the molecules with the energy of the water molecules. The calculation shows that the  $\eta^1$ -mode of binding (**IV**) of catechol is found to be energetically much more stable than  $\eta^2$ -binding modes (**V** and **VI**) by 12.9 and 94.2 kcal mol<sup>-1</sup>, respectively, in the gas phase. Single-point solvent calculations were also performed by using the CPCM<sup>[31]</sup> approach, which is an implementation of the conductor-like screening solvation model (COSMO)<sup>[32]</sup> in Gaussian 03; THF was used as solvent (dielectric constant = 7.58). The calculation shows that the  $\eta^1$ -mode of binding (**IV**) of catechol is also energetically more stable than  $\eta^2$ -binding modes (**V** and **VI**) by 58.1 and 79.6 kcal mol<sup>-1</sup>, respectively. No geometry optimizations were performed for any of these molecules.

**Supporting Information** (see footnote on the first page of this article): Cyclic voltammograms of  $\text{Fe}^{\text{III}}(\text{OEP})(\text{Hcat})$  and  $\text{Fe}^{\text{III}}(\text{OEP})(\text{sal})$  (Figure S1).

## Acknowledgments

We are thankful to the Department of Science and Technology, Government of India and the Council of Scientific and Industrial Research (CSIR), India for financial support. A. C. and R. P. thank CSIR, India for their fellowships.

- [1] a) Y. Watanabe, H. Nakajima, T. Ueno, *Acc. Chem. Res.* **2007**, *40*, 554–562; b) Y. Watanabe, H. Fujii, in *Metal-Oxo and Metal-Peroxo Species in Catalytic Oxidations* (Ed.: B. Meunier), Springer, New York, **2000**, vol. 97, pp. 61–89.
- [2] a) H. P. Hersleth, U. Ryde, P. Rydberg, C. H. Görbitz, K. K. Andersson, *J. Inorg. Biochem.* **2006**, *100*, 460–476; b) H. B. Dunford, *Heme Peroxidases*, Wiley-VCH, New York, **1999**.
- [3] a) H. N. Kirkman, G. F. Gaetani, *Trends Biochem. Sci.* **2007**, *32*, 44–50; b) G. R. Schonbaum, B. Chance, in *The Enzymes* (Ed.: P. D. Boyer), Academic Press, New York, **1976**, vol. 13, pp. 363–408.
- [4] C. D. Putnam, A. S. Arvai, Y. Bourne, J. A. Tainer, *J. Mol. Biol.* **2000**, *296*, 295–309.
- [5] P. Chelikani, I. Fita, P. C. Loewen, *Cell Mol. Life Sci.* **2004**, *61*, 192–208.
- [6] M. T. Green, *J. Am. Chem. Soc.* **2001**, *123*, 9218–9219.
- [7] A. Takahashi, T. Kurahashi, H. Fujii, *Inorg. Chem.* **2009**, *48*, 2614–2625.
- [8] a) D. Kanamori, Y. Yamada, A. Onoda, T. Okamura, S. Adachi, H. Yamamoto, N. Ueyama, *Inorg. Chim. Acta* **2005**, *358*, 331–338; b) N. Ueyama, N. Nishikawa, Y. Yamada, T. Okamura, A. Nakamura, *Inorg. Chim. Acta* **1998**, *283*, 91–97; c) M. P. Byrn, C. J. Curtis, Y. Hsiou, S. Khan, P. A. Sawin, S. K. Tendick, A. Terzis, C. E. Strouse, *J. Am. Chem. Soc.* **1993**, *115*, 9480–9497; d) A. M. Helms, W. D. Jones, G. L. McLendon, *J. Coord. Chem.* **1991**, *23*, 351–355; e) R. D. Arasasingham, A. L. Balch, C. R. Cornman, J. S. de Ropp, K. Eguchi, G. N. La Mar, *Inorg. Chem.* **1990**, *29*, 1847–1850; f) H. Sugimoto, N. Ueda, M. Mori, *Chem. Lett.* **1982**, 449–452.
- [9] a) R. D. Arasasingham, A. L. Balch, R. L. Hart, L. Latos-Grazynski, *J. Am. Chem. Soc.* **1990**, *112*, 7566–7571; b) A. L. Balch, R. L. Hart, L. Latos-Grazynski, *Inorg. Chem.* **1990**, *29*, 3253–3256; c) S. L. Kessel, D. N. Hendrickson, *Inorg. Chem.* **1980**, *19*, 1883–1889.
- [10] L. Cheng, M. A. Khan, D. R. Powell, R. W. Taylor, G. B. Richter-Addo, *Chem. Commun.* **1999**, 1941–1942.
- [11] a) H. Fujii, Y. Funahashi, *Angew. Chem. Int. Ed.* **2002**, *41*, 3638–3641; b) M. I. Davis, A. M. Orville, F. Neese, J. M. Zaleski, J. D. Lipscomb, E. I. Solomon, *J. Am. Chem. Soc.* **2002**, *124*, 602–614; c) E. I. Solomon, T. Brunold, M. I. Davis, J. N. Kemsley, S.-K. Lee, N. Lehnert, F. Neese, A. J. Skulan, Y.-S. Yang, J. Zhou, *Chem. Rev.* **2000**, *100*, 235–349; d) L. Que, R. Y. N. Ho Jr., *Chem. Rev.* **1996**, *96*, 2607–2624; e) A. L. Feig, S. J. Lippard, *Chem. Rev.* **1994**, *94*, 759–805.
- [12] a) G. Du, A. Ellern, L. K. Woo, *Inorg. Chem.* **2004**, *43*, 2379–2386; b) G. D. Fallon, S. J. Langford, M. A.-P. Lee, E. Lygris, *Inorg. Chem. Commun.* **2002**, *5*, 715–718; c) A. Tutass, M. Klopfer, H. Huckstadt, U. Cornelissen, H. Homborg, *Z. Anorg. Allg. Chem.* **2002**, *5*, 1027; d) M. Kurihara, N. Katoh, T. Kojima, Y. Ishii, Y. Matsuda, *Inorg. Chem.* **1995**, *34*, 4888–4895.
- [13] a) J. L. Sessler, A. Mozaffari, M. R. Johnson, *Org. Synth.* **1992**, *70*, 68–78; b) B. Cheng, J. D. Hobbs, P. G. Debrunner, J. Erlebacher, J. A. Shelnut, W. R. Scheidt, *Inorg. Chem.* **1995**, *34*, 102–110.
- [14] T. Uno, K. Hatano, Y. Nishimura, Y. Arata, *Inorg. Chem.* **1990**, *29*, 2803–2807.
- [15] S. K. Sur, *J. Magn. Reson.* **1989**, *82*, 169–173.
- [16] E. T. Kintner, J. H. Dawson, *Inorg. Chem.* **1991**, *30*, 4892–4897.
- [17] K. Nakamura, A. Ikezaki, Y. Ohgo, T. Ikeue, S. Neya, M. Nakamura, *Inorg. Chem.* **2008**, *47*, 10299–10307.
- [18] a) R. Patra, A. Chaudhary, S. K. Ghosh, S. P. Rath, *Inorg. Chem.* **2010**, *49*, 2057–2067; b) R. Patra, S. Bhowmik, S. K. Ghosh, S. P. Rath, *Dalton Trans.* **2010**, *39*, 5795–5806; c) S. K. Ghosh, R. Patra, S. P. Rath, *Inorg. Chem.* **2010**, *49*, 3449–3460; d) S. K. Ghosh, R. Patra, S. P. Rath, *Inorg. Chim. Acta* **2010**, *363*, 2791–2799; e) R. Patra, A. Chaudhary, S. K. Ghosh, S. P. Rath, *Inorg. Chem.* **2008**, *47*, 8324–8335; f) S. K. Ghosh, R. Patra, S. P. Rath, *Inorg. Chem.* **2008**, *47*, 10196–10198.
- [19] M. J. Frisch, G. W. Trucks, H. B. Schlegel, G. E. Scuseria, M. A. Robb, J. R. Cheeseman, J. A. Montgomery Jr., T. Vreven, K. N. Kudin, J. C. Burant, J. M. Millam, S. S. Iyengar, J. Tomasi, V. Barone, B. Mennucci, M. Cossi, G. Scalmani, N. Rega, G. A. Petersson, H. Nakatsuji, M. Hada, M. Ehara, K. Toyota, R. Fukuda, J. Hasegawa, M. Ishida, T. Nakajima, Y. Honda, O. Kitao, H. Nakai, M. Klene, X. Li, J. E. Knox, H. P. Hratchian, J. B. Cross, V. Bakken, C. Adamo, J. Jaramillo, R. Gomperts, R. E. Stratmann, O. Yazyev, A. J. Austin, R. Cammi, C. Pomelli, J. W. Ochterski, P. Y. Ayala, K. Morokuma, G. A. Voth, P. Salvador, J. J. Dannenberg, V. G. Zakrzewski, S. Dapprich, A. D. Daniels, M. C. Strain, O. Farkas, D. K. Malick, A. D. Rabuck, K. Raghavachari, J. B. Foresman, J. V. Ortiz, Q. Cui, A. G. Baboul, S. Clifford, J. Cioslowski, B. B. Stefanov, G. Liu, A. Liashenko, P. Piskorz, L. Komaromi, R. L.

- Martin, D. J. Fox, T. Keith, M. A. Al-Laham, C. Y. Peng, A. Nanayakkara, M. Challacombe, P. M. W. Gill, B. Johnson, W. Chen, M. W. Wong, C. Gonzalez, J. A. Pople, *Gaussian 03*, revision B.04, Gaussian, Inc., Pittsburgh, PA, **2003**.
- [20] a) N. Ueyama, N. Nishikawa, Y. Yamada, T. Okamura, S. Oka, H. Sakurai, A. Nakamura, *Inorg. Chem.* **1998**, *37*, 2415–2421; b) N. Ueyama, N. Nishikawa, Y. Yamada, T. Okamura, A. Nakamura, *J. Am. Chem. Soc.* **1996**, *118*, 12826–12827.
- [21] a) S. Floquet, A. J. Simaan, E. Riviere, M. Nierlich, P. Thuery, J. Enslin, P. Gutlich, J.-J. Girerd, M.-L. Boillot, *Dalton Trans.* **2005**, 1734–1742; b) A. J. Simaan, M.-L. Boillot, R. Carrasco, J. Cano, J. J. Girerd, T. A. Mattioli, J. Enslin, H. Spiering, P. Gutlich, *Chem. Eur. J.* **2005**, *11*, 1779–1793; c) M. Higuchi, Y. Hitomi, H. Minami, T. Tanaka, T. Funabiki, *Inorg. Chem.* **2005**, *44*, 8810–8821; d) M. Merkel, D. Schnieders, S. M. Baldeau, B. Krebs, *Eur. J. Inorg. Chem.* **2004**, 783–790.
- [22] a) T. Wada, M. Yamanaka, T. Fujihara, Y. Miyazato, K. Tanaka, *Inorg. Chem.* **2006**, *45*, 8887–8894; b) P. B. Kettler, Y.-D. Chang, J. Zubietta, M. J. Abrams, *Inorg. Chim. Acta* **1994**, *218*, 157–165; c) A. Vlcek, *Comments Inorg. Chem.* **1994**, *16*, 207–228; d) S. Bhattacharya, S. R. Boone, G. A. Fox, C. G. Pierpont, *J. Am. Chem. Soc.* **1990**, *112*, 1088–1096.
- [23] Z. Pan, D. N. Harischandra, M. Newcomb, *J. Inorg. Biochem.* **2009**, *103*, 174–181.
- [24] a) H. Hirao, S. Shaik, P. M. Kozlowski, *J. Phys. Chem. A* **2006**, *110*, 6091–6099; b) L.-C. Xu, Z.-Y. Li, T.-J. He, F.-C. Liu, D.-M. Chen, *Chem. Phys.* **2004**, *305*, 165–174; c) T. Vangberg, R. Lie, A. Ghosh, *J. Am. Chem. Soc.* **2002**, *124*, 8122–8130; d) K. Prendergast, T. G. Spiro, *J. Phys. Chem.* **1991**, *95*, 9728–9736.
- [25] A. D. Adler, F. R. Lango, F. Kampas, *J. Inorg. Nucl. Chem.* **1970**, *32*, 2443–2445.
- [26] *SAINT+*, version 6.02., Bruker AXS, Madison, WI, **1999**.
- [27] G. M. Sheldrick, *SADABS 2.0*, **2000**.
- [28] G. M. Sheldrick, *SHELXL-97: Program for Crystal Structure Refinement*, University of Göttingen, Göttingen, Germany, **1997**.
- [29] A. D. Becke, *J. Chem. Phys.* **1993**, *98*, 5648–5652.
- [30] C. Lee, W. Yang, R. G. Parr, *Phys. Rev. B* **1988**, *37*, 785–789.
- [31] a) V. Barone, M. Cossi, *J. Phys. Chem. A* **1998**, *102*, 1995–2001; b) M. Cossi, N. Rega, G. Scalmani, V. Barone, *J. Comput. Chem.* **2003**, *24*, 669–681.
- [32] a) A. Klamt, G. Schürmann, *J. Chem. Soc. Perkin Trans. 2* **1993**, 799–805; b) A. Schäfer, A. Klamt, D. Sattel, J. C. W. Lohrenz, F. Eckert, *Phys. Chem. Chem. Phys.* **2000**, *2*, 2187–2193.

Received: June 29, 2010  
Published Online: October 19, 2010